This is the Pre-Published Version.

Iridium motif linked porphyrins for efficient light-driven hydrogen evolution via triplet state stabilization of porphyrin

Daniel Nnaemaka Tritton,[‡a] Govardhana Babu Bodedla,[‡a] Geliang Tang,[b] Jianzhang Zhao,[b] Chak-Shing Kwan,[a] Ken Cham-Fai Leung,*[a] Wai-Yeung Wong*[a,c] and Xunjin Zhu*[a]

Two new iridium motif linked porphyrins, **MBPyZnP-Ir** and **TBPyZnP-Ir** are developed for photocatalytic hydrogen evolution (PHE). The tetra-iridium linked one, **TBPyZnP-Ir**, displayed the highest H_2 production rate (ηH_2) of 16.12 mmol g^{-1} h^{-1} within 5 h of irradiation, which is over 2.73-fold higher than **MBPyZnP-Ir** (5.90 mmol g^{-1} h^{-1}) and much higher than their precursors **TBPyZnP** (0.12 mmol g^{-1} h^{-1}) and **MBPyZnP** (0.06 mmol g^{-1} h^{-1}) without iridium. The superior ηH_2 of **TBPyZnP-Ir** could be explained by the iridium motifs linked to the porphyrin, stabilizing the triplet states of the porphyrin through intramolecular energy transfer; thus enhancing electron transfer from the triplet photo-excited porphyrin moiety to the cobaloxime co-catalyst and consequently proton reduction.

Introduction

Since fossil fuels are a finite resource, and contribute to greenhouse effects through carbon emissions, the world faces an unprecedented energy crisis, as well as extreme weather changes with disastrous side effects. Therefore, new technologies must be developed to produce energy in an environmentally clean, economical and efficient manner.[1,2] Plants convert sunlight and carbon dioxide (CO_2) to chemicals via photosynthesis, during which they produce oxygen (O_2) and carbohydrates.[3] By mimicking natural photosynthetic pathways, the development of artificial photosynthesis to produce hydrogen (H_2) as a renewable energy source is fundamental in creating a clean energy system.[4] Since the first photo-electrochemical cell (PEC) for splitting water was developed by Fujishima and Honda,[5] many efforts have been given to developing diverse and effective photocatalytic H_2 evolution (PHE) systems.[6,7]

Except for those widely investigated metal oxides and graphitic carbon nitrides, carbon-based semiconductors, transition metal complexes and organic dyes have also been studied as photosensitizers for PHE.[8] Metal complexes based on iridium (Ir(III)) are exceptional candidates for PHE, in terms of photophysical properties such as long emission lifetime, high Stokes shift, good photostability, electrochemical versatility and tunability.[7,8c, 9-15] Recently, Wang et al. reported an Ir complex, decorated with coumarins, linked to bodipy for use as a highly efficient photosenitizer in hydrogen evolution; whereby the Ir(III) center acts as a mediator between the two fluorophores and enhances the T_1 state of bodipy through heavy atom effect, therefore rapidly improving photocatalytic hydrogen evolution.[16] On the other hand, systems based on porphyrin have received growing attention in recent years due to their vast variety of structures and key roles in biology, particularly photocatalysis and artificial photosynthesis.[17] Porphyrins and their metal complexes display an intense absorption in the visible region of the solar spectrum, possess high chemical and thermal stability and easily tunable photophysical properties.[18-20]

Regardless of the aforementioned, there are only a few multi-metallic systems composed of metallo-porphyrins linked to iridium.[21] One example, reported by Martir et al. is that of a dyad consisting of two zinc(II)-tetraphenylporphyrin (ZnTPP) units and a cyclometalated Ir(III) motif, connected via non-covalent interactions between the zinc (Zn) metal in TPP and pyridine moieties on the Ir motif.[21] There are three examples of systems containing a porphyrin directly conjugated to a transition metal: a TPP group covalently linked to the N atom of a diiron azadithiolate (ADT) moiety,[22] a metal complex dyad containing a Zn porphyrin linked to a rhenium bipyridyl complex, via an amide linkage and Zn-porphyrin containing four tris(4,4'-dimethyl-2,2'-bipyridine)ruthenium(II) complexes as substituents at the *meso* position.[23] The above compounds were characterized and their optoelectronic properties were studied, however no PHE application was investigated. Thus, developing covalently conjugated Ir(III) motif linked to porphyrins could be an ideal strategy to understand the photophysical interaction between the Ir motif and porphyrin core and its potential application in light driven water splitting. It could also be of benefit using such a system that undergoes intersystem crossing transformation of singlet excited state (S_1) to triplet excited state (T_1) upon photoexcitation, since the T_1 state is more stable and longer lived, and hence may provide an increased number of photogenerated electrons for subsequent proton (H^+) reduction to H_2.

[a] *Department of Chemistry. Hong Kong Baptist University, Waterloo Road, Kowloon Tong, Hong Kong, P. R. China. X. Zhu, E-mail: xjzhu@hkbu.edu.hk; cfleung@hkbu.edu.hk.*
[b] *School of Chemical Engineering. Dalian University of Technology. Dalian, China.*
[c] *Department of Applied Biology & Chemical Technology. The Hong Kong Polytechnic University. Hong Kong, P. R. China; The Hong Kong Polytechnic University Shenzhen Research Institute, Shenzhen, 518057, China. wai-yeung.wong@polyu.edu.hk.*
[‡] *These authors contributed equally.*
Electronic Supplementary Information (ESI) available: [Materials and methods, synthesis, photocatalytic systems at different conditions, emission spectra and emission decay profiles, Jablonski energy diagram, cyclic voltammograms, ^1H and ^{13}C NMR spectra, MALDI–TOF spectrum]. See DOI: 10.1039/x0xx00000x

Herein, we report two new Ir(III) motif linked porphyrins **MBPyZnP-Ir** and **TBPyZnP-Ir** for use in PHE. The Ir(III) motif itself produced long lifetime triplet states upon light irradiation, meanwhile, stabalized the triplet state of the porphyrin by intramolecular energy transfer, consequently improving electron transfer from the triplet photo-excited both Ir(III) and porphyrin moiety to the chloro(pyridine)cobaloxime (**CoPyCl**) co-catalyst. As a result, an impressive PHE capability with a rate of 16.12 mmol g^{-1} h^{-1} was achieved, which is 16 times higher than that of the typical porphyrin derivative coupled with Pt co-catalyst reported previously.[19]

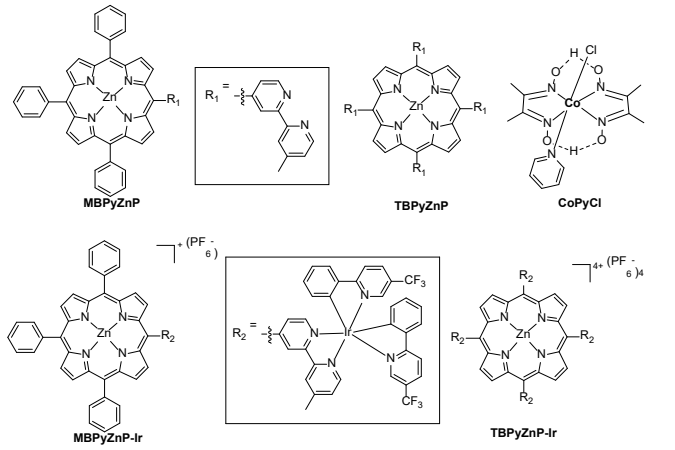

Fig. 1 Structures of **MBPyZnP**, **TBPyZnP**, **MBPyZnP-Ir**, **TBPyZnP-Ir** and **CoPyCl**.

Results and discussions

Optoelectronic properties

The synthesis of bipyridine (BPy) substituted porphyrins (**MBPyZnP** and **TBPyZnP**) and Ir(III) motif-linked porphyrins (**MBPyZnP-Ir** and **TBPyZnP-Ir**) is illustrated in Scheme S1 (See ESI). All the new compounds were confirmed by spectroscopic methods including ^{1}H and ^{13}C NMR, and MALDI-TOF MS.

The absorption spectra of the porphyrins recorded in acetonitrile (MeCN) are shown in Fig. 2(a). The weak peaks located at *ca.* 230-320 nm, intense peaks at *ca*. 400-450 nm and weaker set of peaks at *ca*. 520 nm - 620 nm are attributed to aromatic rings in the entire complex structures, the Ir(III) motif, Soret bands and the Q-bands of the porphyrin, respectively. The Ir(III) motif linked to the porphyrins results in strong absorption in the UV regions from Ir(III) motif, and broad red-shifted Soret and Q bands, besides, the peaks of **MBPyZnP-Ir** are shifted by *ca*. 5 nm and **TBPyZnP-Ir** shifted by *ca*. 20 nm possibly due to aggregation effect. Typically, **TBPyZnP-Ir** shows absorption from 220 to 720 nm which could act as a good photosensitizer to harvest photons in the entire UV-visible region. Upon the excitation at $\lambda \geq 400$ nm, **MBPyZnP** and **TBPyZnP** in aerated or degassed MeCN at 298 K showed very similar vibronic-structured emission with λ_{max} at 610 and 655 nm (Fig. S1 in ESI). The decay of the emission at 610 nm for **MBPyZnP** in aerated solution has a single-exponential nanosecond fluorescence decay of 7.2 ns, while the same emission peak in degassed solution shows a characteristic biexponential behaviour containing a prompt constituent with a lifetime of 233 ns and a delayed constituent with a lifetime of 6379 ns (Fig. S2 & S3 in ESI). The results indicate the existence of thermally activated delayed fluorescence (TADF) for **MBPyZnP** in which there is a steric hindrance between the electron-donor (porphyrin core) and electron-acceptor (BPy) segments.

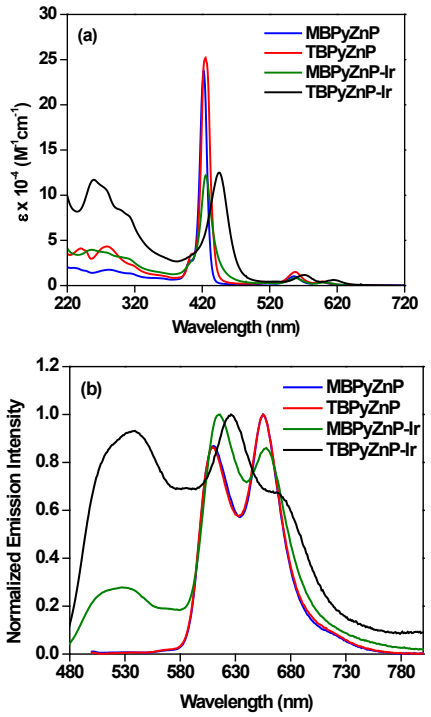

Fig. 2 (a) Absorption and (b) emission spectra of the porphyrins recorded in MeCN (10 μM) at room temperature.

Moreover, the small ΔE_{ST} of 0.15 eV between the calculated singlet state and triplet state will cause **MBPyZnP** to realize a reverse intersystem crossing (RISC) process and thus exhibit TADF behavior (Fig. S4 in ESI). Similarly, the emission at 610 nm for **TBPyZnP** displays biexponential fluorescence decay of 243 ns and 6650 ns (Fig. S5 in ESI), corresponding to TADF behavior. In contrast, the Ir(III) linked porphyrins **MBPyZnP-Ir** and **TBPyZnP-Ir** show dual-emissive behaviour with a higher-energy Gaussian emission band centered at *ca*. 520–525 nm in addition to the vibronic-structured emission at *ca*. 615–670 nm (Fig. 2(b)). In addition, excitation-dependent emission spectra support the existence of two distinctive emissive excited states, whereas the relative emission intensity of the porphyrin emission increases as the excitation wavelength moves closer to the Soret band of the porphyrin (Fig. S6 and S7 in ESI). The lifetimes of the Gaussian bands are also found to be in the microsecond regime, confirming their triplet origin. The emission is assigned as originated from the admixture of ^{3}IL[π→π*(phenylpyridine and bipyridine)] and ^{3}MLCT[dπ(Ir)→π*(phenylpyridine and bipyridine)] excited states. It is found that **TBPyZnP-Ir** displays a more intense Ir(III) emission band than that of **MBPyZnP-Ir**, which is in line with the increased number of Ir moieties. When compared with **MBPyZnP-Ir**, the emission is slightly red-shifted for **TBPyZnP-Ir**,

which was reflected in its narrower HOMO - LUMO gap in cyclic voltammetry study (*vide infra*). The emission and absorption data are summarized in Table 1. The fluorescence lifetime (τ_F) and quantum yield (Φ_F) of each compound was calculated and summarized in Table 1.

On the other side, the excitation at a wavelength (250 nm) within the absorption range of Ir(III) motif clearly populates emission peaks from porphyrin ring (Fig. S6 in ESI). In addition, the porphyrin shows strong absorption in the range of 500-720 nm and overlapped with the emission of Ir(III) motif within 480-600 nm, hence allowing for efficient intramolecular energy transfer between the Ir(III) motif energy donor and the porphyrin energy acceptor (Fig. S8 in ESI). Given these results, the partial efficient energy transfer from the Ir(III) motif to the porphyrin ring for both **MBPyZnP-Ir** and **TBPyZnP-Ir** should be beneficial for efficiently harvesting solar light harvesting, stabilizing excited states of porphyrin, as well as enhancing PHE rate (*vide infra*).

Table 1. Photophysical data of the porphyrins recorded in MeCN solution.

Compound	Medium (T / K)	λ_{abs} (ε x 10^4)	λ_{max} / nm (τ_o / μs)	$\Phi_{PL(Soln)}$ [a]
MBPyZnP	MeCN (298)	281 (1.75), 422 (2.37), 556 (1.02), 597 (0.40)	610, 655 (0.23, 6.4)	0.033
TBPyZnP	MeCN (298)	240 (4.11), 279 (4.33), 425 (2.52), 558 (1.50), 598 (0.44)	610, 655 (0.30, 7.4)	0.025
MBPyZnP-Ir	MeCN (298)	256 (3.96), 425 (1.22), 558 (0.83), 599 (0.34)	520 (1.1), 615, 658	< 0.01
TBPyZnP-Ir	MeCN (298)	260 (1.17), 445 (1.25), 571 (1.17), 615 (0.63)	535 (1.1), 626, 670	< 0.01

[a]The luminescence quantum yield, measured at room temperature using $[Ru(bpy)_3]Cl_2$ in degassed MeCN solution as the reference (excitation wavelength = 436 nm, Φ_{lum} = 0.06).

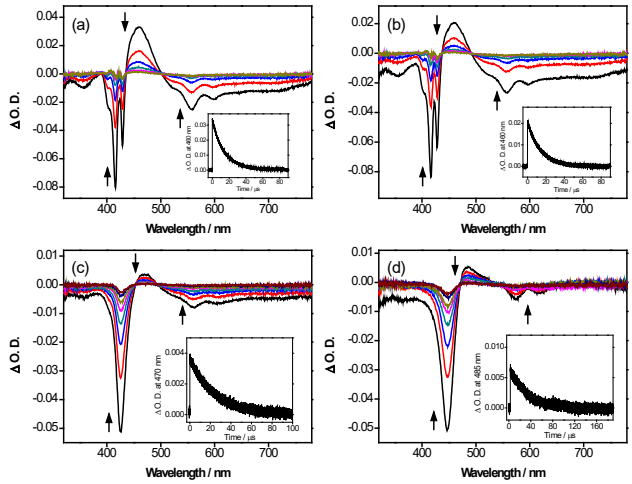

Fig. 3 Transient absorption difference spectra of (a) **MBPyZnP** and (b) **TBPyZnP** in MeCN (1×10^{-5} M) at room temperature at decay times of 0–50 μs with time intervals of 10 μs. Inset shows the decay trace of the absorptions monitored at 460 nm; (c) **MBPyZnP-Ir** in MeCN (1×10^{-5} M) at room temperature at decay times of 0–80 μs with time intervals of 20 μs. Inset shows the decay trace of the absorptions monitored at 475 nm; (d) **TBPyZnP-Ir** in CH_3CN (1×10^{-5} M) at room temperature at decay times of 0–70 μs with time intervals of 10 μs. Inset shows the decay trace of the absorptions monitored at 485 nm.

To obtain more information on the nature of the excited states of the porphyrin complexes, nanosecond transient absorption (TA) measurements were performed on compounds **MBPyZnP**, **TBPyZnP**, **MBPyZnP-Ir**, **TBPyZnP-Ir** in degassed MeCN solution at room temperature. The TA difference spectra of the compounds determined at different delay times after a 355 nm laser pulse excitation and the respective decay traces are shown in Fig. 3(a)-(d). All compounds exhibit an intense negative band at *ca.* 415 nm to 446 nm, corresponding to the ground-state bleach resulting in the diminution of the Soret band of the porphyrin ring, and a moderately intense positive excited-state absorption band at *ca.* 460 to 485 nm. The bleaching signals at *ca*. 540 nm are tentatively assigned to the ground state Q band absorption of the porphyrin ring. The decay lifetimes of all compounds are found to be in the microsecond regime, confirming the T_1 origin of the excited states. The decay lifetimes of all compounds are summarized in Table 2. It is worth noting that the excited-state lifetimes of the porphyrin in **MBPyZnP-Ir** and **TBPyZnP-Ir** are higher than that of the counterparts (**MBPyZnP** and **TBPyZnP**) without Ir(III) motif. More importantly, **TBPyZnP-Ir** is also found to possess longer excited-state lifetimes than that of **MBPyZnP-Ir**. These results are indicative of the fact that intersystem crossing from S_1 to T_1 excited state occurs for the porphyrin ring and suggest that the Ir(III) motif linked to porphyrin core would stabilize the T_1 excited state of the porphyrin; additionally Ir(III) may enhance the intersystem crossing through the heavy atom effect. Such T_1 stabilization and heavy atom contribution will increase the number of photogenerated electrons that are excited from S_0 ground state to S_1 excited state and subsequently transferred to T_1 excited state, which can be further used to reduce Co (from +3 to +1) center in **CoPyCl** co-catalyst and initiate proton reduction to H_2.

The redox potentials of the porphyrins were measured by performing cyclic voltammetry experiments (Fig. S9 and Table 2). As shown in Fig. 4, the excited state reduction potential (E_{red}*) values of the porphyrins are more positive than the oxidation potential (E_{ox}) of triethylamine (TEA), while the excited state oxidation potential (E_{ox}*) values of porphyrins are more negative than the reduction potential (E_{red}) of **CoPyCl**. This suggests a favorable thermodynamic driving force for accepting

electrons from TEA as sacrificial donor in the excited state of porphyrins and an effective transfer of electrons from photoexcited porphyrins to **CoPyCl** co-catalyst. Moreover, these results further indicate that the photocatalytic process could be assigned to a reductive quenching mechanism. More importantly, the tetra Ir(III) conjugated porphyrin **TBPyZnP-Ir** features the deepest low-lying E_{ox}* energy level in the series (Fig. 4), which would likely produce higher PHE efficiency.

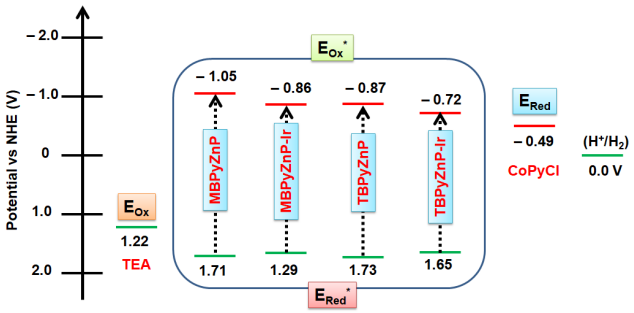

Fig. 4 Energy level alignment of the porphyrins, sacrificial donor and co-catalyst.

Table 2. Nanosecond transient absorption and electrochemical data of the porphyrins.

Compound	Medium (T / K)	λ_{max} (nm)	τ_o (µs)	E_{Ox}, V [a] (vs NHE)	E_{Red}, V [b] (vs NHE)	E_{Ox}*, V [c] (vs NHE)	E_{red}*, V [d] (vs NHE)	$E_{0\text{-}0}$ [e]
MBPyZnP	MeCN (298)	415, 425 460	12.9 14.3	1.16, 1.54,	– 0.50, – 1.05	– 1.05,	1.71	2.21
TBPyZnP	MeCN (298)	415, 425 460	13.8 14.3	1.29, 1.80	– 0.49, – 0.99	– 0.86	1.66	2.15
MBPyZnP-Ir	MeCN (298)	426 470	23.8 24.4	1.35, 1.82,	– 0.49, – 1.04	– 0.87	1.73	2.22
TBPyZnP-Ir	MeCN (298)	446 485	29.9 32.7	1.40, 1.80, 1.22	– 0.47, – 1.08 -	– 0.72 -	1.65 -	2.12 -
CoPyCl [f]				-	-	– 0.49, – 0.86	-	-

[a] The oxidation potentials of the porphyrins, TEA and CoPyCl were recorded in MeCN (100 µM) with 0.1 M $TBAPF_6$ as electrolyte (working electrode: glassy carbon; counter electrode: Pt wire; reference electrode: non-aqueous Ag/Ag+; ferrocene was used as internal standard for potential calibration). [b] E_{Red} (vs NHE) = 0.77 + E_{red} (vs Ferrocene) [c] E_{Ox}* (vs NHE) = E_{Ox} – $E_{0\text{-}0}$. [d] E_{Red}* (vs NHE) = E_{Red} + $E_{0\text{-}0}$. [e] Estimated from the intersection of the normalized absorption and emission spectra. [f] The literature value was converted from SCE to NHE by adding + 0.244 V.

Photocatalytic hydrogen evolution (PHE) studies

The PHE studies were evaluated by the photocatalytic systems (PSs) using the porphyrins as a photosensitizer, **CoPyCl** as a co-catalyst, triethylamine (TEA) as a sacrificial electron donor, and H_2O as a proton source. The PHE results of all the porphyrins are shown in Fig. 5 and summarized in Table 3. Under the optimized conditions, the PSs of Ir(III) motif linked porphyrins **TBPyZnP-Ir** (ηH_2 = 16.12 mmol g^{-1} h^{-1} and AQE = 2.38) and **MBPyZnP-Ir** (ηH_2 = 5.90 mmol g^{-1} h^{-1} and AQE = 0.42) gave high PHE results compared to those of porphyrins **TBPyZnP** (ηH_2 = 0.12 mmol g^{-1} h^{-1} and AQE = 0.01) and **MBPyZnP** (ηH_2 = 0.06 mmol g^{-1} h^{-1}) without the Ir(III) motif under the light irradiation of 5 h. The better PHE results of Ir(III) linked porphyrins could be ascribed to their high light harvesting capability in the entire UV-visible, intramolecular energy transfer from Ir(III) motifs to the porphyrin, low-lying E_{ox}* energy levels, stabilized T_1 excited state and efficient photogenerated charge carrier's separation (Fig. S10 & S11 ESI).[24] The order of turnover number (TON) of the porphyrins is as follws: **TBPyZnP-Ir** (246.0) > **MBPyZnP-Ir** (82.17) > **TBPyZnP** (2.58) > **MBPyZnP** (1.92). The porphyrins with Ir(III) motifs are also showing good photostability attested by their continuously increment in PHE up to 40 h of light irradiation (Fig. 5b). To give an insight into how to optimize the PHE systems, we tested all four compounds for H_2 whilst varying the solvent ratio of MeCN/H_2O and varying the concentration of TEA (for **TBPyZnP-Ir**) and **CoPyCl** co-catalyst (for **MBPyZnP-Ir** and **TBPyZnP-Ir**) (Fig. S12-S14). All four porphyrins displayed a lower ηH_2 when changing the solvent ratio of MeCN/H_2O from 2:1 v/v to 1:2 v/v, respectively; **TBPyZnP-Ir** displayed a gradual increase in ηH_2 when increasing the concentration of TEA from 0.08–0.8 M; **MBPyZnP-Ir** and **TBPyZnP-Ir** both exhibited a lower ηH_2 when reducing the concentration of **CoPyCl** from 0.4 mM to 0.2 mM. These results indicate the importance of organic solvent/H_2O ratio and co-catalyst concentration on optimizing the performance of the photocatalytic system to generate H_2; the PHE conditions stated in Fig. 5 gave the most efficient HER for all four porphyrins. The ηH_2 production was also tested whilst varying the concentration of **TBPyZnP-Ir** from 0.5-100 µM was shown to give the highest production rate (Fig. S15), thus giving more insight into how to optimize the PSs.

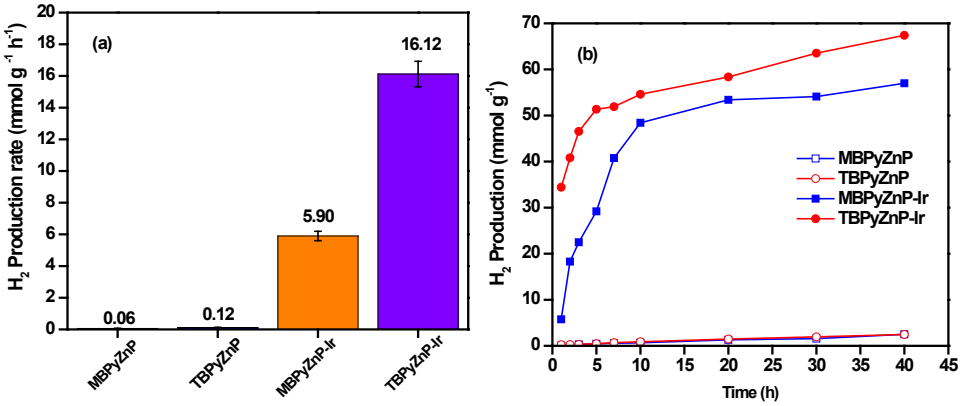

Fig. 5 (a) H_2 production rate of photocatalytic systems under the irradiation for 5 h and (b) H_2 production of photocatalytic systems under the irradiation for 40 h: (Photosensitizer (0.1 mM) + TEA (0.8 M) + **CoPyCl** (0.4 mM) + MeCN/H_2O (2:1 v/v)).

Table 3. H_2 production rate (ηH_2), apparent quantum efficiency (AQE) and turnover number (TON) data of photocatalytic systems.

Compound	ηH_2 (mmol g^{-1} h^{-1})[a]	TON[b]	AQE (%)[c]
MBPyZnP	0.06	1.92	-
TBPyZnP	0.12	2.58	0.01
MBPyZnP-Ir	5.90	82.17	0.42
TBPyZnP-Ir	16.12	246.00	2.38

[a,c] Calculated under irradiation for 5 h. [b] Calculated for 40 h.

A proposed photo-redox mechanism for **MBPyZnP-Ir** and **TBPyZnP-Ir** displayed in Fig. 6. After photoexcitation by LED white light, the light was absorbed by the Ir(III)-containing porphyrins (denoted ZnPor-Ir in Fig. S12 in ESI), followed by conversion of S_1 excited state to T_1 excited state through the intersystem crossing (mediated by Ir(III) through heavy atom effect). The T_1 state of ZnPor-Ir then accepted an electron from TEA to give the reduced $[ZnP\text{-}Ir]^-$ species, which could in turn donate 2 electrons to reduce Co(III)PyCl to Co(I)PyCl; with the Co(I) species ultimately being used to reduce protons to H_2, with high efficiency. More importantly, the stability of PSs also could be improved by tetra Ir(III) motif linked to the porphyrin.

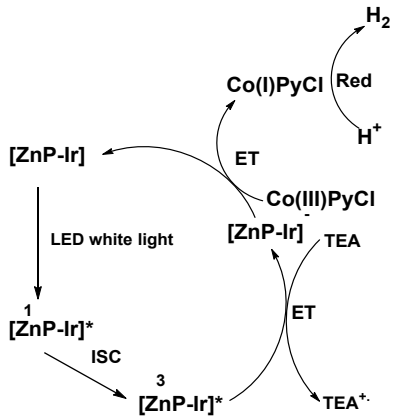

Fig. 6 Proposed electron transfer mechanism and photo-redox cycle for PHE with ZnP-Ir (MBPyZnP-Ir and TBPyZnP-Ir). Zn is coordination center, Ir is iridium antenna, ET is electron transfer, ISC is intersystem crossing and Red is reduction.

To study the electron transfer mechanism in our PHE system, phosphorescence quenching experiments of **MBPyZnP-Ir** were performed by varying the concentrations of CoPyCl and TEA, respectively. The Stern-volmer quenching constants (K_q) of **MBPyZnP-Ir** by CoPyCl and TEA were found to be 1.6 x 10^2 M^{-1} and 4.58 M^{-1}, respectively (Fig. S10). These results suggest that the Zn coordination center in MBPyZnP-Ir can efficiently accept an electron from TEA, and the phosphorescence of MBPyZnP-Ir can also be effectively quenched by CoPyCl. Given the concentration of TEA (0.8 M) is much higher than for CoPyCl (0.4 mM) in our photocatalytic system, the photocatalytic pathway should be determined as the reductive quenching mechanism;[25,26] in this process, the iridium containing porphyrin (ZnP-Ir) absorbs light, giving an excited Zn center. The excited Zn complex then accepts an electron from TEA to produce a reduced Zn species, which further reduces Co(III) (in **CoPyCl**) to Co(I) through a multi-electron transfer mechanism, thereby evolving H_2.

Conclusions

In conclusion, iridium motifs linked porphyrins **MBPyZnP-Ir** and **TBPyZnP-Ir** were prepared from the precursors **MBPyZnP**, **TBPyZnP**, respectively. TA analysis reveal that the Ir(III) motif linked to porphyrin increases the T_1 lifetime, indicating the stabilization of the triplet excited states of the porphyrin, therefore improved H_2 evolution. As expected, **TBPyZnP-Ir** gave the highest PHE results compared to **MBPyZnP-Ir**, and their precursors without Ir(III), **MBPyZnP** and **TBPyZnP**. The higher performance of **TBPyZnP-Ir**, is attributed to the deep low lying E_{ox}* energy levels, intramolecular energy transfer, and a higher number of photogenerated electrons, efficient transfer of electrons from the excited state porphyrins to the co-catalyst, and thus proton reduction; as well as enhancement of intersystem crossing by the heavy atom effect from Ir(III). This concept would be further optimized in future work involving porphyrin-based materials to improve their light-driven H_2 evolution and CO_2 reduction.

Conflicts of interest

There are no conflicts to declare.

Acknowledgements

This study was supported by Hong Kong Baptist University (FRG2-16-17-024, FRG2-17-18-068, RC-ICRS/15-16/02E, RC-ICRS/1617/02C-CHE, RC-IRMS/16/17/02CHEM), the State Key Laboratory of Environmental and Biological Analysis as well as The President's Award for Outstanding Performance in Research Supervision to K.C.-F.L.. W.-Y. Wong. acknowledges the financial support from Hong Kong Research Grants Council (PolyU 153051/17P), the National Natural Science Foundation of China (51873176), the Hong Kong Polytechnic University (1-ZE1C) and Ms. Clarea Au for the Endowed Professorship in Energy (847S). Lastly, we appreciated Dr. K.-W. Kong and Prof. Vivian W.-W. Yam from The University of Hong Kong for TA measurements and analysis.

Notes and references

1. H. N. Kagalwala, E. Gottlieb, G. Li, T. Li, R. Jin and S. Bernhard, *Inorg. Chem.,* 2013, **52**, 9094-9101.
2. N. D. McDaniel and S. Bernhard, *Dalton Trans.,* 2010, **39**, 10021-10030.
3. M. Watanabe, *Sci. Technol. Adv. Mater.,* 2017, **18**, 705-723.
4. (a) H. Yi, T. Peng, D. Ke, D. Ke, L. Zan and C. Yan, *Int. J. Hydrogen Energy,* 2008, **33**, 672-678; (b) Y. Kuramochi, A. S. D. Sandanayaka, A. Satake, Y. Araki, K. Ogawa, O. Ito and Y. Kobuke, *Chem. Eur. J.,* 2009, **15**, 2317-2327.
5. A. Fujishima and K. Honda, *Nature*, 1972, **238**, 37-38.
6. (a) B. B. Beyene and C.-H. Hung, *Sustainable Energy Fuels,* 2018, **2**, 2036-2043; (b) D. B. Vasilchenko, S. V. Tkachev, A. Y. Kurenkova, E. A. Kozlova and D. V. Kozlov, *Int. J. Hydrog. Energy,* 2016, **41**, 2592-2597.
7. (a) V. Balzani, A. Credi and M. Venturi, *ChemSusChem,* 2008, **1**, 26-58; (b) M. Kirch, J.-M. Lehn and J.-P. Sauvage, *Helv. Chim. Acta,* 1979, **62**, 1345-1384.
8. (a) Y. Xu, Y. Huang and B. Zhang, *Inorg. Chem. Front.,* 2016, **3,** 591-615; (b) P. Kumar, R. Boukherroub and K. Shankar, *J. Mater. Chem. A,* 2018, **6**, 12876-12931; (c) Y.-J. Yuan, Z.-T. Yu, D.-Q. Chen and Z.-G. Zou, *Chem. Soc. Rev.,* 2017, **46**, 603-631; (d) M. Wang, Y. Na, M. Gorlov and L. Sun, *Dalton Trans.*, 2009, 6458–6467; (e) M. Watanabe, *Sci. Technol. Adv. Mater*., 2017, **18**, 705-723; (f) X. Zhang, T. Peng and S. Song, *J. Mater. Chem. A*, 2016, **4**, 2365-2402; (g) M. Wang, Y. Yang, J. Shen, J. Jiang and L. Sun, *Sustainable Energy Fuels*, 2017, **1**, 1641–1663; (h) J. Wen, J. Xie, X. Chen, X. Li, *Appl. Surf. Sci.,* 2017, **391**, 72–123.
9. Y. Ma, H. Liang, Y. Zeng, H. Yang, C.-L. Ho, W. Xu, Q. Zhao, W. Huang and W.-Y. Wong, *Chem. Sci.,* 2016, **7**, 3338-3346.
10. H. Sun, S. Liu, W. Lin, K. Y. Zhang, W. Lv, X. Huang, F. Huo, H. Yang, G. Jenkins, Q. Zhao and W. Huang, *Nat. Commun.*, 2014, **5**, 3601.
11. Z. Chen, Z. Bian and C. Huang, *Adv. Mater.,* 2010, **22**, 1534-1539.
12. C. Lentz, O. Schott, T. Auvray, G. Hanan and B. Elias, *Inorg. Chem*., 2017, **56**, 10875-10881.
13. B. F. DiSalle and S. Bernhard, *J. Am. Chem. Soc.,* 2011, **133**, 11819-11821.
14. L. L. Tinker, N. D. McDaniel, P. N. Curtin, C. K. Smith, M. J. Ireland and S. Bernhard, *Chem. Eur. J*., 2007, **13**, 8726-8732.
15. A. Fihri, V. Artero, A. Pereira and M. Fontecave, *Dalton Trans.,* 2008, **41**, 5567-5569.
16. P. Wang, S. Guo, H.-J. Wang, K.-K. Chen, N. Zhang, Z.-M. Zhang and T.-B. Lu, *Nat. Commun.,* 2019, **10**, 3155.
17. (12) S. Schmidbauer, A. Hohenleutner and B. König, *Beilstein J. Org. Chem.,* 2013, **9**, 2088-2096.
18. Y.-J. Yuan, D. Chen, J. Zhong, L.-X. Yang, J.-J. Wang, Z.-T. Yu and Z.-G. Zou, *J. Phys. Chem. C,* 2017, **121**, 24452-24462.
19 G. B. Bodedla, L. Li, Y. Che, Y. Jiang, J. Huang, J. Zhao and X. Zhu, *Chem. Commun.*, 2018, **54**, 11614-11617.
20. L. Li, G. B. Bodedla, Z. Liu and X. Zhu, *Appl. Surf. Sci.*, 2020, **499**, 143755.
21. D. R. Martir, G. J. Hedley, D. B. Cordes, A. M. Z. Slawin, D. Escudero, D. Jacquemin, T. Kosikova, D. Philp, D. M. Dawson, S. E. Ashbrook, I. D. W. Samuel and E. Zysman-Colman, *Dalton Trans.,* 2016, **45,** 17195-17205.
22. L. C. Song, M. Y. Tang, F. H. Su and Q. M. Hu, *Angew. Chem. Int. Ed.,* 2006, **45**, 1130-1133.
23. (a) Y. Kou, S. Nakatani, G. Sunagawa, Y. Tachikawa, D. Masui, T. Shimada, S. Takagi, D. A. Tryk, Y. Nabetani, H. Tachibana and H. Inoue, *J. Catal.,* 2013, **310**, 57-66; (b) K. Araki, P. Losco, F. M. Engelmann, H. Winnischofer and H. E. Toma, *J. Photochem. Photobiol. A,* 2001, **142**, 25-30.
24. S. Fan, X. Zong, P. E. Shaw, X. Wang, Y. Geng, A. R. G. Smith, P. L. Burn and L. Wang, S.-C. Lo, *Phys. Chem. Chem. Phys.,* 2014, **16**, 21577-21585.
25. N. Zhang, K.-K. Chen, S. Guo, P. Wang, M. Zhang, J. Zhao, Z.-M. Zhang, T.-B. Lu, *Appl. Catal. B,* 2019, **253**, 105-110.
26. Q. Luo, R. Ge, S.-Z. Kang, L. Qin, G. Li, X. Li, *Appl. Surf. Sci.* 2018, **427**, 15-23.